IEEE Photonics Journal
An IEEE Photonics Society Publication

Fiber Optic Magnetic Field Sensor Based on Magnetic Nanoparticle Assembly in Microcapillary Ring Resonator

Volume 9, Number 5, October 2017

Zhe Yu
Junfeng Jiang
Xuezhi Zhang
Kun Liu
Shuang Wang
Wenjie Chen
Tiegen Liu

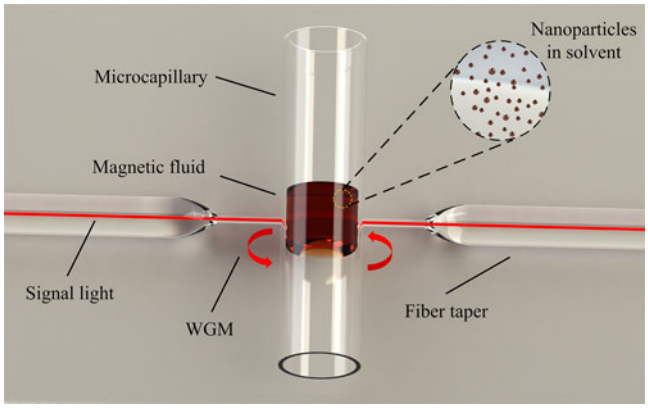

DOI: 10.1109/JPHOT.2017.2756822
1943-0655 © 2017 IEEE

Fiber Optic Magnetic Field Sensor Based on Magnetic Nanoparticle Assembly in Microcapillary Ring Resonator

Zhe Yu, Junfeng Jiang, Xuezhi Zhang, Kun Liu, Shuang Wang, Wenjie Chen, and Tiegen Liu

School of Precision Instrument and Opto-Electronics Engineering, Institute of Optical Fiber Sensing of Tianjin University, Tianjin Optical Fiber Sensing Engineering Center, Key Laboratory of Opto-Electronics Information Technology, Tianjin University, Tianjin 300072, China

DOI:10.1109/JPHOT.2017.2756822

Manuscript received August 22, 2017; accepted September 21, 2017. Date of publication September 26, 2017; date of current version October 9, 2017. This work was supported in part by the National Natural Science Foundation of China under Grants 61675152, 61378043, 61405139, 61475114, 61505139, and 61505138 and in part by the National Instrumentation Program of China under Grant 2013YQ030915.
Corresponding authors: Junfeng Jiang and Xuezhi Zhang (jiangjfjxu@tju.edu.cn; Zhangxz@tju.edu.cn).

Abstract: A magnetic field sensor based on the magnetic-field-induced nanoparticle assembly effect in microcapillary whispering gallery mode (WGM) ring resonator is proposed and experimentally demonstrated. The chemical characteristics of nanoparticles and the silica microcapillary are used to link up the surface density of the resonator and the magnetic field intensity. The magnetic field variation changes the surface density of nanoparticles adsorbed on the sensor surface and respond to the WGM transmission spectra shift. Because of the powerful surface sensing capability of WGM, the maximum sensing sensitivity reaches 57.59 nm/mT and the detection limit reaches 1.39×10^{-4}, respectively. The magnetic field response characteristic of the sensor is studied as well. This provides the potential to fiber-based magnetic field sensing applications.

Index Terms: Fiber-optic sensor, magnetic field sensing, whispering gallery mode, nanoparticle assembly.

1. Introduction

Magnetic field sensors have been widely used in the field of navigation, aerospace, geophysics, engineering as well as medical science etc. [1], [2]. Fiber-optic magnetic-field sensors have attracted a lot of attention these years owing to their remarkable advantages such as electromagnetic interference immunity, compactness, high resolution and resistance to high pressure and corrosion [3]. Owing to the small Verdet constant of silica fiber, sensors based on Faraday effect [4] of the fiber itself needs a long fiber to achieve a decent response. Therefore, most of the fiber-optic magnetic-field sensors are achieved by combining silica fiber and magnetic functional materials such as magnetostrictive materials [5] and magneto-optical materials [6]. The former requires the difficult mechanical bonding of magnetostrictive material to optical fiber and has low reliability due to mechanical deformation, by contrast, the latter depends on refractive index (RI) change of magneto-optical materials and are more frequently used.

Magnetic fluid (MF) is a special magneto-optical material, which is a colloidal solution composing of solvent and magnetic nanoparticles. Thus, MF possesses the property of magnetic-induced RI change [7] and the fluidity makes it easier to be integrated with fibers. Different configurations of fiber optic magnetic field sensors based on magnetic fluid have been proposed, such as multimode interference structure [8], [9], Mach–Zehnder interferometer [10], microfiber knot resonator [11], fiber taper [12], Dual-S-Shaped fiber [13], hollow core fiber [14] and so on. However, those sensors work with the bulk RI change of magnetic fluid under external magnetic field, the order of magnitude for the variation in RI is 10^{-3}. In 2004, Hong *et al*. [15] reported that the RI of magnetic fluid increased from 1.4352 to 1.5062 as the concentration of magnetic nanoparticles in the magnetic fluid rose from 1.21% to 1.93%, this indicates that the concentration-induced RI shift is more obvious than magneto-optic effect of magnetic fluid. For a certain magnetic fluid, the average concentration of nanoparticle is established, but the local concentration distribution can also be influence by magnetic field, this effect is usually used in the separation of biologic samples [16] and drug delivery [17]. To manipulate the local concentration distribution will provide a chance to enhance the magnetic sensing sensitivity. The concentration of nanoparticle adsorbed on the sensor surface, which is often expressed as surface density, is easy to manipulate as the surface will provide the nanoparticles with forces, such as electrostatic force and hydrogen bonding. Whispering gallery mode (WGM) [18] is an effective surface sensing mechanism and obtain excellent sensing properties in fluid composition detection applications [19], [20]. Recent years, the researches [21]–[24] on WGM combining with magnetic nanoparticle are mainly due to the high photo-thermal effect of MF, which presents an all-optical WGM resonance wavelength tuning approach by employing an optical pump. The application on magnetic field sensing is reported by Mahmood *et al*. [25], [26], the sensor is formed by magnetic fluid infiltrated photonic crystal fiber WGM resonator and the resonance wavelength can respond the magnetic field. However, this sensor is still based on magnetic induced bulk RI variation and the magnetic-field sensitivity is only 0.1 nm/mT. The previous researches on WGM combining with magnetic nanoparticle overlook the chemical characteristics of nanoparticles and the resonator, which can develop the powerful surface sensing capability of WGM.

In this work, we propose and investigate a fiber optic magnetic field sensor based on micro-capillary WGM ring resonator combining with magnetic fluid. We take advantage of the chemical characteristics of the silica microcapillary and the PEG-coated nanoparticle, make the nanoparticle adsorbed on the surface of resonator. The applied magnetic field can separate the nanoparticles from the surface to assemble to chain in the direction of magnetic field in solution. The powerful surface sensing capability of WGM is very sensitive to the surface density change of the resonator and reflects on the resonator wavelength. The new mechanism we adopt in this paper improve the magnetic field sensitivity to 57.59 nm/mT. To the best of our knowledge, this is the highest sensitivity achieved by fiber-optic magnetic field sensor.

2. Sensing Principle

Fig. 1 shows the schematic diagram of the sensor. The WGM is excited in the wall of a microcapillary ring resonator by a fiber taper. The microcapillary is filled with magnetic fluid. The nanoparticle in magnetic fluid is Fe_3O_4 coated with polyethyene glycol (PEG). The PEG polymer layer has uncharged hydrophilic residues and very high surface mobility [27], leading to high steric exclusion which offers an available method to prevent aggregation between nanoparticles. In addition to this, there is abundant hydroxyl group (-OH) [28] on the surface of PEG layer with chemical activity.

As shown in Fig. 2(a), the silica microcapillary can also carry a significant number (around $2.5\mathrm{OH}/\mathrm{nm}^2$) of silanol group (Si-OH) after a surface activation process with NaOH [29], [30]. PEG−silica hydrogen bonding [31] is easy to form between hydroxyl group and silanol group. Under the effect of hydrogen bonding, most of the nanoparticles in magnetic fluid will be absorbed on the surface of the microcapillary, then the local concentration near surface increases greatly. The WGM is confined in the evanescent field which also exits near the microcapillary surface. The high-concentration region and the evanescent field almost has a complete overlap and produces

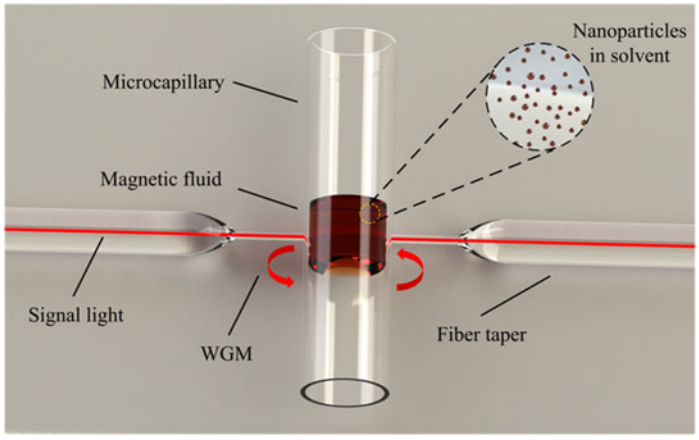

Fig. 1. A schematic illustration of the magnetic field sensor. The brown spherical nanoparticles dispersed in the solvent represent Fe_3O_4 nanoparticles in the magnetic fluid.

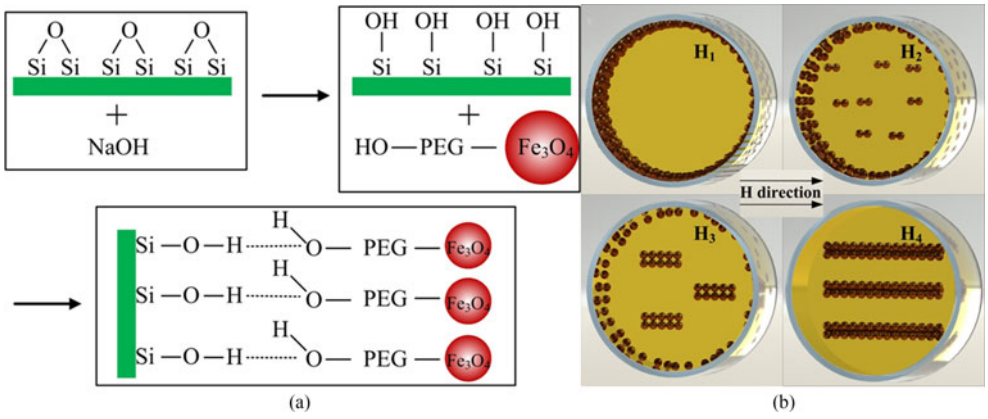

Fig. 2. (a) Diagram of the forming process of PEG−silica hydrogen bonding. The green square represents the silica microcapillary wall. (b) Diagram of the distribution change of nanoparticles under an increasing external magnetic field from H_1 to H_4. The arrow indicate the direction of the external magnetic field.

much higher light-matter interaction efficiency than other fiber optic sensor method, thus realizing a very high sensing sensitivity.

From Fig. 2(b), we can see that when external magnetic field is applied to the sensor, the magnetic-field-induced nanoparticle assembly effect [32] begins to work. The nanoparticles gradually moved under the magnetic field to aggregate into nanochains in the field direction [33]. With the increase of the magnetic field intensity, more nanoparticles will escape from the wall as the hydrogen bond can't counteract the magnetic force. The nanochains will absorb more nanoparticles to grow longer and also aggregate into string-like clusters [34]. Finally, when the magnetic field intensity reaches a certain threshold every adsorbed nanoparticle will escape from the wall and became part of the magnetic clusters in the solvent. The decrease of nanoparticle concentration near the surface will greatly change the local RI and reflect in the WGM spectra.

The WGM spectra shift can be expressed as [35]

$$\frac{\delta\lambda}{\lambda} = \sigma_P \alpha_{ex} \frac{2\pi\sqrt{n_2^2 - n_1^2}}{\varepsilon_0 \lambda^2} \frac{n_2}{n_1^2} S \tag{1}$$

where $\delta\lambda$ is the WGM spectral shift, σ_p is the surface density of the nanopartical that deposits on the surface, α_{ex} is the excess polarizability, n_1 (1.33) is the RI of aqueous medium in the resonator

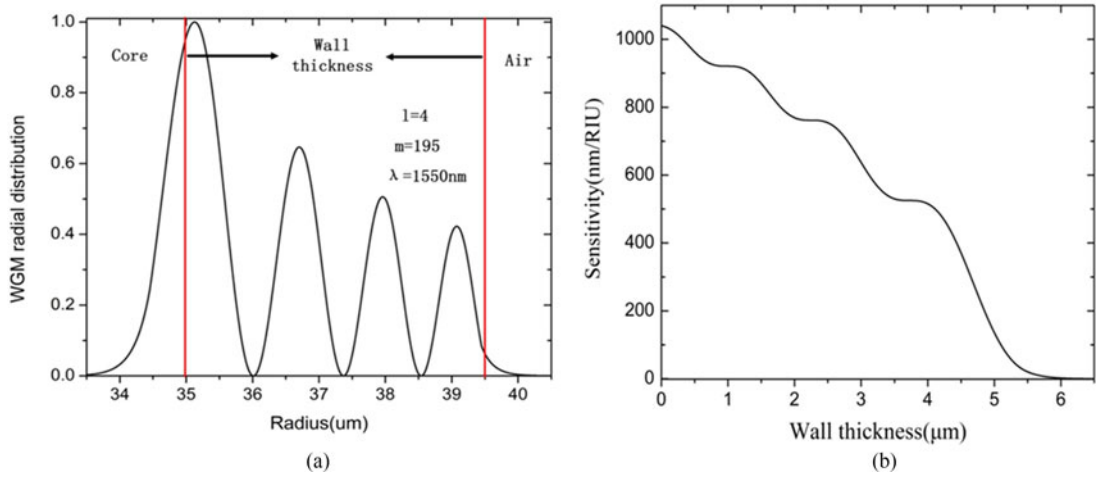

Fig. 3. (a) Intensity distribution of the TM^4_{195} WGM mode ($\lambda = 1550$ nm), the red line represents the inner and outer surfaces of the capillary and separates the core, wall and the surrounding medium air. (b) Calculated bulk RI sensitivity dependence on the wall thickness of microcapillary with the diameter of 78.9 μm.

and n_2 (1.45) is the RI of the ring resonator wall, ε_0 (8.85×10^{-12} F/m) is the vacuum permittivity, S is the bulk RI sensitivity of the device, and λ (1550 nm) is the wavelength of the WGM spectra. Considering the known parameters and summarizing them to a constant k, the (1) can be simplified as

$$\delta\lambda = k\Delta\sigma_P\alpha_{ex}S \tag{2}$$

For an iron-oxide magnetic nanoparticles with 5 nm diameter, the excess polarizability α_{ex} is estimated to be $(4\pi\varepsilon_0)\,2.53 \times 10^{-18}\,cm^3$ [36]. The bulk RI sensitivity S is mainly decided by the distribution proportion of the light energy in the resonator core [18]. Fig. 3(a) shows a TM^4_{195} WGM mode under 1550 nm of a ring resonator with the diameter of 78.9 μm, which is calculated by Mie theory [37]. The optical and the structure parameters are same as in the experiment. The light energy of a WGM mode exists both in the resonator wall and core, only the light exposed in the core is sensitive to the RI change of the analyte, thus decides the sensitivity. Fig. 3(b) shows an inverse relationship between the sensitivity and the wall thickness, as the light energy distributed in the resonator core increases with the reduction of the wall thickness. The wall thickness should be reduced as small as possible to enlarge the bulk RI sensitivity S. So we adopt a pressured pulling technology to obtain a thin wall microcapillary.

The surface density σ_p is decided by the number of nanoparticles adsorbed on the sensor surface. In the absence of external field, the σ_p reaches the maximum and it decreases with the applying of the magnetic field. Defining the magnetic field strength as H, then σ_p can be expressed as an H-related function $\sigma_p(H)$. We arrive at

$$\delta\lambda = k\Delta\sigma_P(H)\alpha_{ex}S \tag{3}$$

For a certain sensor, the excess polarizability α_{ex} of nanoparticle and bulk RI sensitivity S of resonator won't change with the magnetic field. The surface density variation $\Delta\sigma_p(H)$ is directly reflected in the WGM spectral shift $\delta\lambda$, which bring about the magnetic field sensing by spectra measurement.

3. Experimental Results and Discussion

A commercial fused silica capillary (TSP250350, Polymicro Inc.) is processed to establish the ring resonator. We first reduce the wall thickness to increase sensitivity according to the theoretical

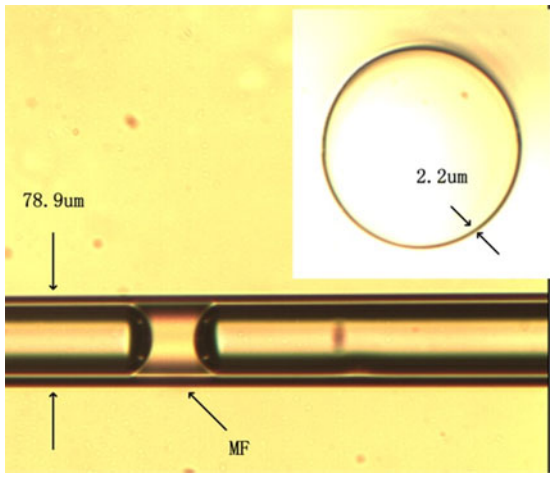

Fig. 4. The side and cross-sectional view of the thin wall silica capillary, the outer diameter is 78.9 μm and the wall thickness is 2.2 μm.

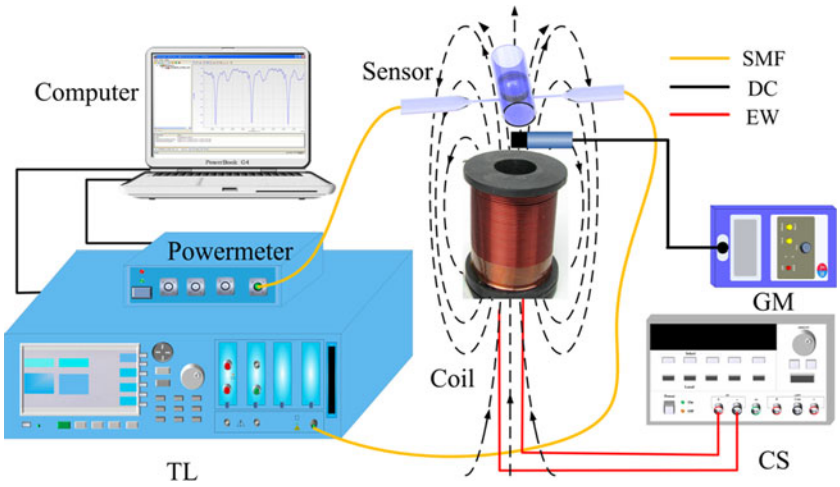

Fig. 5. Schematic diagram of the experimental setup for investigating the properties of the sensor. TL: tunable laser, CS: current source, GM: Gauss meter, SMF: single-mode fibre, DC: data cable, EW: electric wire.

analysis. The silica capillary is locally heated under oxyhydrogen flame, and is drawn by a motorized stage when it is heated to fuse. Pressurized air (101.380 Kpa, 55 Kpa larger than atmospheric pressure) is pumped through the capillary to avoid capillary collapse and decrease the wall thickness while keep the smooth surface quality. The diameter of the silica capillary is reduced from 360 μm to 78.9 μm. As shown in Fig. 4, the wall thickness of the capillary can be as thin as 2.2 μm. A fiber taper with 2 μm diameter is also fabricated by the flame-heated stretching technique. The capillary and the fiber taper are separately fixed on tunable bracket and are adjusted under the help of microscope to ensure precise vertical of their axial orientation and achieve high coupling efficiency. The capillary is rinsed with 1.0 M NaOH for 2 h to activate the surface Si-OH, and then washed with deionized water for 5 min. The activated capillary is filled with magnetic fluid (from Cytodiagnostics Inc.), which contains water-soluble iron-oxide magnetic nanoparticles with 5 nm diameter. The concentration of the MF is 5 mg/ml.

Fig. 5 shows the experimental setup for investigating the properties of the sensor. A tunable laser (TL) with a resolution of 0.1 pm is connected to the fiber taper of the sensor as a laser source. The light transiting the fiber taper is coupled into the capillary by the evanescent wave, generating

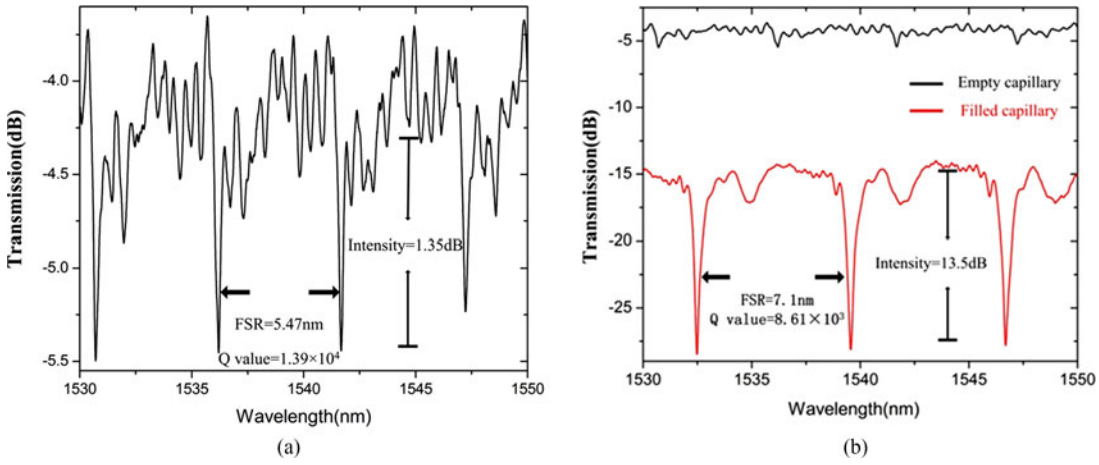

Fig. 6. (a) Transmission spectra of an empty capillary, the FSR is 5.47 nm, the Q value is 1.39 $\times$ 10^4 and the peak intensity is 1.35 dB. Fig. 5. (b) Black line indicates the transmission spectrum of empty capillary, red line indicates the transmission spectrum after MF injection. The FSR of the filled capillary is 7.1 nm, the Q value is 8.61 $\times$ 10^3 and the peak intensity is 13.5 dB.

WGM in capillary. An optical powermeter (PM) is connected to the other end of the fiber taper to measure the transmission spectrμm. The tunable laser and powermeter are connected with a computer control platform to acquire and process the WGM spectra. A magnetic coil is used to generate the magnetic field, the field direction is perpendicular to the fiber axis and the microcapillary axis. The diameter of the coil diameter(8 cm) is much larger than the sensor, and the distance between the sensor and the coil is about 1.1 mm (the thickness of the glass slide to support the coil), so the magnetic field can be seen as constant in direction during the experiment. The strength of the applied field is controlled by changing the output of a DC current source (CS). A Gauss meter (GM) probe is placed between the coil and the sensor in the gap of two glass slides to monitor the magnetic field intensity. The measurement of peak wavelength is repeated ten times and averaged.

We first measure the transmission spectrum when the capillary is empty without filling MF. As shown in Fig. 6, the free spectral range (FSR) is 5.47 nm for an empty capillary, and it increases to 7.1 nm after the capillary is filled with magnetic fluid. That's because the RI of water-based magnetic fluid (n $=$ 1.33) is larger than air (n $=$ 1), and the FSR of WGM spectra is proportion to the effective RI of the resonator when the radius of resonator is fixed. After the injection of MF, the Q factor of resonator peaks decrease from 1.39 $\times$ 10^4 to 8.61 $\times$ 10^3, the transmission loss of resonator peaks increase sharply and the resonance peak intensity has multiplied from 1.35 dB to 13.5 dB. It is due to the effect of PEG$-$silica hydrogen bonding between the silica capillary and the nanoparticles in MF, which get the nanoparticles self-assemble on the surface of capillary and form a nanoparticle layer, the evanescent field energy distribution in the layer is absorbed to a large extent by the iron-oxide nanoparticle.

Fig. 7 illustrates the WGM spectra of the sensor under the magnetic field of 0.068 mT, 0.075 mT, 0.083 mT, 0.090 mT and 0.098 mT, respectively. It can be seen that with the increase of the magnetic field, the spectra experience a blue shift. However, in many researches it is generally recognized that the spectra shows a red shift when the magnetic field intensity increases. The difference is that the microcapillary is treated on surface for the activation of silicon hydroxyl, then the PEG –coated nanoparticles in MF can be assembled on the surface of microcapillary under the effect of PEG$-$silica hydrogen bonding, just like a high-index layer which reflects on the large resonant wavelength. When the external magnetic field is applied on the sensor, the nanoparticles begin to separate from the surface on account of magnetic force as they tend to assemble to chain in the direction of magnetic field. The increasement of the applied magnetic field leads to a sustained reduction of surface density σ_p, as well reduces the resonator wavelengths of the sensor according to the theoretical analysis.

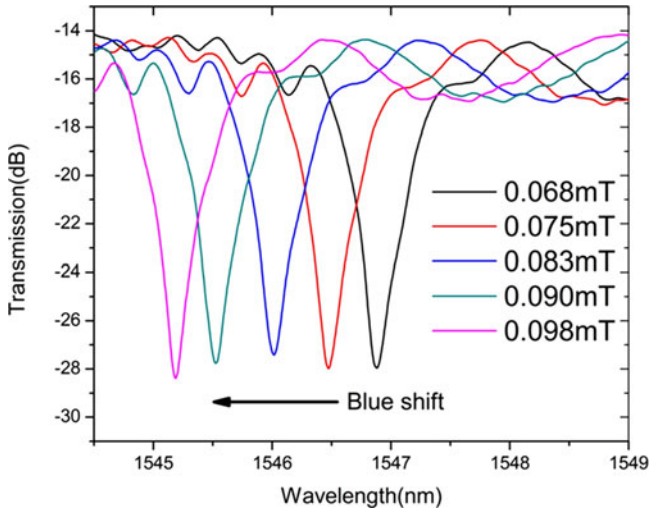

Fig. 7. Transmission spectra of the sensor under magnetic-field intensity of 0.068 mT, 0.075 mT, 0.083 mT, 0.090 mT and 0.098 mT, with the increase of magnetic field, the spectra experience a blue shift.

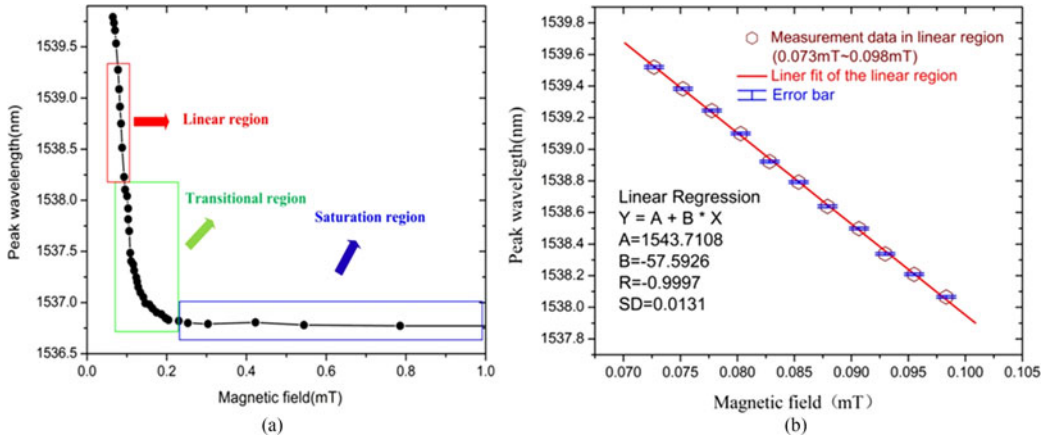

Fig. 8. (a) WGM resonance wavelength versus applied magnetic field, the process is devided into 3 sections as linear region, transitional region and saturation region. Fig. 7. (b) Liner fit of the sensitivity in the linear region (from 0.073 mT to 0.098 mT). The green diamond with blue error bar is the experiment measurement, the red line is the liner fit result.

Fig. 8(a) shows the WGM resonance wavelength versus applied magnetic field. For clarity, we divide the process into 3 sections as linear region, transitional region and saturation region, respectively. It can be seen that the resonance wavelength changes rapidly in the linear region, because under small magnetic field intensity, the magnetic force and hydrogen bonding are comparable, the nanoparticles separate from the wall at a relatively uniform speed. As the magnetic field continue to increase, it goes into transitional region, the resonance wavelength changes slower with the increasing of magnetic field intensity, which also means the sensitivity of the sensor is reduced. That's due to a majority of the nanoparticles have fall into the solution, the number of separated nanoparticle under each magnetic field intensity become smaller and smaller. When the magnetic field intensity reaches saturation region, the resonance wavelength doesn't change with the increasing of magnetic field intensity any more. The magnetic field intensity reaches the threshold that the magnetic force become considerably larger than the effect of PEG–silica hydrogen bonding, all the surface adsorbed nanoparticles are pulled down and aggregate into string-like

clusters in the solution. Thus, the surface density of the resonator keeps as a constant and so as the resonance wavelength.

Fig. 8(b) shows the zoomed linear region and it gives the maximum sensitivity. The red line is the linear fit result of the liner region, the sensitivity reaches a value as high as 57.59 nm/mT in the magnetic field intensity range from 0.073 mT to 0.098 mT. The absolute value of the linearly dependent coefficient reaches 0.9997 and the standard deviation of the fit is as low as 0.0131, which indicates a good linearity. The WGM peak wavelength measuring fluctuation is about 8 pm, which can represent the minimμm distinguishable peak shift of the sensor, thus the detection limit of this sensor is 1.39×10^{-4}mT. The sensitivity of this sensor is at least 2 order of magnitude higher than the reported WGM-based fiber optic magnetic field sensors and 1 order of magnitude higher than the reported other fiber optic magnetic field sensors.

4. Conclusion

In conclusion, a high sensitivity magnetic field sensor based on magnetic-field-induced nanoparticle assembly and surface sensing capability of microcapillary WGM ring resonator is proposed. The magnetic field response characteristic is observed and explained by the feature of the MF and the processed silica microcapillary. The WGM transmission spectra shift with the variation of the external magnetic-field intensity has been studied in detail. The maximum sensing sensitivity reaches 57.59 nm/mT and the detection limit reaches 1.39×10^{-4} in consideration of the resolution. Due to its high sensitivity, compact size and low-cost fabrication process, this sensor would find potential applications in the measurement of magnetic field.

Acknowledgment

The authors would like to thank the anonymous reviewers for their valuable suggestions.

References

[1] P. Ripka, Magnetic Sensors and Magnetometers. Boston, MA: Artech House, 2001.
[2] J. Lenz and A. S. Edelstein, "Magnetic sensors and their applications," *IEEE Sensors J.*, vol. 6, no. 3, pp. 631–649, Jun. 2006.
[3] Y. Chen, Q. Han, T. Liu, X. Lan, and H. Xiao, "Optical fiber magnetic field sensor based on single-mode-multimode-single-mode structure and magnetic fluid," *Opt. Lett.*, vol. 38, no. 20, pp. 3999–4001, 2013.
[4] L. Sun, S. Jiang, and R. J. Marciante, "All-fiber optical magnetic-field sensor based on Faraday rotation in highly terbium-doped fiber," *Opt. Exp.*, vol. 18, no. 6, pp. 5407–5412, 2010.
[5] Y. Du, T. Liu, Z. Ding, K. Liu, B. Feng, and J. Jiang, "Distributed magnetic field sensor based on magnetostriction using Rayleigh backscattering spectra shift in optical frequency-domain reflectometry," *Appl. Phys. Exp.*, vol. 8, no. 1, p. 012401, 2015.
[6] I. M. White and X. Fan, "On the performance quantification of resonant refractive index sensors," *Opt. Exp.*, vol. 16, no. 2, pp. 1020–1028, 2008.
[7] P. Zu *et al.*, "Magneto-optical fiber sensor based on magnetic fluid," *Opt. Lett.*, vol. 37, no. 3, pp. 398–400, 2012.
[8] Y. Chen, Q. Han, T. Liu, X. Lan, and H. Xiao, "Optical fiber magnetic field sensor based on single-mode-multimode-single-mode structure and magnetic fluid," *Opt. Lett.*, vol. 38, no. 20, pp. 3999–4001, 2013.
[9] W. Lin, Y. Miao, H. Zhang, B. Liu, Y. Liu, and B. Song, "Fiber-optic in-line magnetic field sensor based on the magnetic fluid and multimode interference effects," *Appl. Phys. Lett.*, vol. 103, no. 15, 2013, Art. no. 151101.
[10] P. Zu *et al.*, "Temperature-insensitive magnetic field sensor based on nanoparticle magnetic fluid and photonic crystal fiber," *IEEE Photon. J.*, vol. 4, no. 2, pp. 491–498, Apr. 2012.
[11] X. Li and H. Ding, "All-fiber magnetic-field sensor based on microfiber knot resonator and magnetic fluid," *Opt. Lett.*, vol. 37, no. 24, pp. 5187–5189, 2012.
[12] L. Luo, S. Pu, J. Tang, X. Zeng, and M. Lahoubi, "Reflective all-fiber magnetic field sensor based on microfiber and magnetic fluid," *Opt. Exp.*, vol. 23, no. 14, pp. 18133–18142, 2015.
[13] X. Q. Lei, B. J. Peng, D. R. Chen, Q. G. Shi, and X. W. Ma, "An all-fiber magnetic field sensor based on dual-s-shaped optic fiber integrated with magnetic fluid," *IEEE Sens. J.*, vol. 16, no. 4, pp. 958–964, Feb. 2015.
[14] B. Song *et al.*, "Loss-Based magnetic field sensor employing hollow core fiber and magnetic fluid," *IEEE Photon. Technol. Lett.*, vol. 26, no. 22, pp. 2283–2286, Nov. 2014.
[15] C. Y. Hong, H. E. Horng, and S. Y. Yang, "Tunable refractive index of magnetic fluids and its applications," *Phys. Status Solidi*, vol. 1, no. 7, pp. 1604–1609, 2004.
[16] Y. Weizmann, F. Patolsky, E. Katz, and I. Willner, "Amplified DNA sensing and immunosensing by the rotation of functional magnetic particles," *J. Amer. Chem. Soc.*, vol. 125, no. 12, pp. 3452–3454, 2003.

[17] M. Arruebo, R. Fernández-Pacheco, M. R. Ibarra, and J. Santamaría, "Magnetic nanoparticles for drug delivery," *Nano Today*, vol. 2, no. 3, pp. 22–32, 2007.
[18] H. Zhu, I. M. White, J. D. Suter, P. S. Dale, and X. Fan, "Analysis of biomolecule detection with optofluidic ring resonator sensors," *Opt. Exp.*, vol. 15, no. 15, pp. 9139–9146, 2007.
[19] G. Yang, I. M. White, and X. Fan, "An opto-fluidic ring resonator biosensor for the detection of organophosphorus pesticides," *Sens. Actuators B, Chem.*, vol. 133, no. 1, pp. 105–112, 2008.
[20] Y. Sun and X. Fan, "Analysis of ring resonators for chemical vapor sensor development," *Opt. Exp.*, vol. 16, no. 14, pp. 10254–10268, 2008.
[21] Y. Li *et al.*, "Tuning of whispering gallery modes in a magnetic-fluid-infiltrated silica capillary based on lateral pumping scheme," *J. Opt.*, vol. 19, no. 1, 2017, Art. no. 015801.
[22] Y. Liu *et al.*, "All-optical tuning of a magnetic-fluid-filled optofluidic ring resonator," *Lab Chip*, vol. 14, no. 16, pp. 3004–3010, 2014.
[23] P. Zhao, L. Shi, Y. Liu, Z. Wang, S. Pu, and X. Zhang, "Iron-oxide nanoparticles embedded silica microsphere resonator exhibiting broadband all-optical wavelength tunability," *Opt. Lett.*, vol. 39, no. 13, pp. 3845–3848, 2014.
[24] L. Wei *et al.*, "Laser-tuned whispering gallery modes in a solid-core microstructured optical fibre integrated with magnetic fluids," *Sci. Rep.*, vol. 5, 2015, Art. no. 17791.
[25] A. Mahmood, V. Kavungal, S. S. Ahmed, G. Farrell, and Y. Semenova, "Magnetic-field sensor based on whispering-gallery modes in a photonic crystal fiber infiltrated with magnetic fluid," *Opt. Lett.*, vol. 40, no. 21, pp. 4983–4986, 2015.
[26] A. Mahmood *et al.*, "Magnetic field sensing using whispering-gallery modes in a cylindrical microresonator infiltrated with ferronematic liquid crystal," *Opt. Exp.*, vol. 12, no. 1, pp. 3–14, 2017.
[27] Y. Zhang, N. Kohler, and M. Zhang, "Surface modification of superparamagnetic magnetite nanoparticles and their intracellular uptake," *Biomaterials*, vol. 23, no. 7, pp. 1553–1561, 2002.
[28] M. Preari, K. Spinde, J. Lazic, E. Brunner, and K. D. Demadis, "Bioinspired insights into silicic acid stabilization mechanisms: The dominant role of polyethylene glycol-induced hydrogen bonding," *J. Amer. Chem. Soc.*, vol. 136, no. 11, pp. 4236–4244, 2014.
[29] O. H. Lin, H. M. Akil, and Z. A. M. Ishak, "Characterization and properties of activated nanosilica/polypropylene composites with coupling agents," *Polym. Composites*, vol. 30, no. 11, pp. 1693–1700, 2009.
[30] R. Mueller, H. K. Kammler, K. Wegner, and S. E. Pratsinis, "OH surface density of SiO_2 and TiO_2 by thermogravimetric analysis," *Langmuir*, vol. 19, no. 1, pp. 160–165, 2003.
[31] X. Q. Liu, R. Y. Bao, X. J. Wu, W. Yang, B.-H. Xie, and M.-B. Yang, "Temperature induced gelation transition of a fumed silica/PEG shear thickening fluid," *RSC Adv.*, vol. 5, no. 24, pp. 18367–18374, 2015.
[32] H. Wang, Y. B. Sun, Q. W. Chen, Y. F. Yu, and K. Cheng, "Synthesis of carbon-encapsulated superparamagnetic colloidal nanoparticles with magnetic-responsive photonic crystal property," *Dalton Trans.*, vol. 39, no. 40, pp. 9565–9569, 2010.
[33] C. M. Liu, L. Guo, R. M. Wang, Y. Deng, H.-B. Xu, and S. Yang, "Magnetic nanochains of metal formed by assembly of small nanoparticles," *Chem. Commun.*, vol. 23, no. 23, pp. 2726–2727, 2004.
[34] X. Qiao *et al.*, "Magnetorheological Behavior of Polyethyene Glycol-Coated Fe_3O_4 Ferrofluids," *Nihon Reoroji Gakkaishi*, vol. 38, no. 1, pp. 23–30, 2010.
[35] H. Zhu, P. S. Dale, C. W. Caldwell, and X. Fan, "Rapid and label-free detection of breast cancer biomarker CA15-3 in clinical human serum samples with optofluidic ring resonator sensors," *Anal. Chem.*, vol. 81, no. 24, pp. 9858–9865, 2009.
[36] F. Vollmer, D. Braun, and A. Libchaber, "Protein detection by optical shift of a resonant microcavity," *Appl. Phys. Lett.*, vol. 80, no. 21, pp. 4057–4059, 2002.
[37] I. M. White, H. Oveys, and X. Fan, "Liquid-core optical ring-resonator sensors," *Opt. Lett.*, vol. 31, no. 9, pp. 1319–1321, 2006.